Journal Name

ARTICLE

Single oxygen vacancies of $(TiO_2)_{35}$ as a prototype of reduced nanoparticle: Implication to photocatalytic activity

Received 00th January 20xx,
Accepted 00th January 20xx

DOI: 10.1039/x0xx00000x

www.rsc.org/

Sunkyung Kim,[a] Kyoung Chul Ko,[a,b] Jin Yong Lee,*[,a] and Francesc Illas*[,b]

Titanium dioxide (TiO_2), as a semiconductor metal oxide, has been one of the most popular materials studied in the field of photocatalysis. In the present study, the properties of single oxygen vacancies of $(TiO_2)_{35}$, a prototype of anatase nanoparticle, were investigated by DFT calculations. $(TiO_2)_{35}$ is the minimum sized model (~ 2 nm) as bipyramidal nanoparticle with anatase phase and eight {101} facets. All the available oxygen vacancies at various sites according to position, coordination number, and distance from the center atom were examined. The geometric, energetic and electronic properties of the reduced TiO_2 clusters were analyzed by hybrid DFT functionals with different Hartree-Fock exchange ratio (0, 12.5 and 25 %). It was found that the structure of pristine $(TiO_2)_{35}$ is somewhat different from bulk lattice with relatively high surface to volume ratio. Moreover, the particular high (three)-coordinated oxygen atom is energetically most favorable for oxygen vacancy formation from nanoparticle mainly due to substantially high relaxation energy. TiO_2 nanoparticle has low oxygen vacancy formation energy and narrow band gap by defect state, and can be utilized as an efficient photocatalyst material.

Introduction

Titanium dioxide (TiO_2) is an important metal oxide for a number of applications including photocatalysis[1, 2] and solar cells.[3-5] To use solar energy as a sustainable energy source, semiconductors for water splitting photocatalyst have to satisfy demands such as optimal band gap, low cost, nontoxicity, stability, and so on. In spite of excellent properties of TiO_2 as a photocatalytic material, its wide band gap (~ 3.2 eV) leads to low efficiency for visible light absorption. Hence many strategies have been developed to reduce the band gap by means of native defects,[6] chemical doping,[7-10] and point defects.[11-14]

Among three kinds of TiO_2 polymorph (anatase, rutile and brookite), rutile is the most stable bulk phase, while most nanomaterials prefer anatase structure due to the lower surface energy of anatase phase than others.[15-17] Nanoparticles (NPs) show remarkably high catalytic performance compared with bulk phase due to large surface area and quantum confinement effect. Though many results have been reported on the properties of TiO_2 systems, theoretical studies are commonly concerning about periodic bulk or surface models. Compared to TiO_2 bulk, NPs are composed of strained lattices, mixed phases or interfaces with several defects.[18] On the other hand, the isolated TiO_2 clusters, Ti_nO_{2n} ($n < 17$),[10, 19-21] have been investigated to compare their structures and properties with those of the bulk phases. However, the structure of clusters composed of few atoms is substantially different from that of the TiO_2 bulk and the cluster size is too small to explain the experimental observation. Thus, a systematic investigation on geometric and electronic properties of TiO_2 NPs, with enough size to maintain lattice structure and facet, different from bulk or slab surface is challenging and attractive. Our recent study revealed that the calculated cluster $(TiO_2)_{35}$ retained the facets found in nanoparticles studied in experiment,[22] thus clusters smaller in size than $(TiO_2)_{35}$ may not give electronic and optical properties of nanoparticles.

Point defects such as oxygen vacancy (O_v) and titanium interstitial play an important role in photocatalytic reaction. O_v, one neutral oxygen vacancy, provides two excess electrons to TiO_2 system and these electrons are responsible for the reduction of Ti^{4+} to Ti^{3+}. The formation of Ti^{3+} species upon reduced TiO_2 were confirmed by several kinds of experimental observations, such as photoelectron spectroscopy,[23] electron paramagnetic resonance (EPR),[11] and shift in the core level binding energies.[24] The defect states originating from trapped electrons appear around 1.0 eV below the conduction band minimum (CBM), which induces band gap narrowing as optimal value for photocatalyst.[23, 25-27] Many theoretical studies were also conducted about the properties of O_v in TiO_2 system such as O_v in bulk,[9, 28-34] surface and subsurface,[35, 36] and polaronic nature induced by O_v[37-39] using various calculation methods. However, to the best of our knowledge, the property of O_v in isolated system considering the effect of

[a] Department of Chemistry, Sungkyunkwan University, Suwon 16419, Korea. E-mail: jinylee@skku.edu; Phone: +82-31-299-4560; Fax: +82-31-290-7075
[b] Departament de Química Física & Institut de Química Teòrica i Computacional (IQTCUB), Universitat de Barcelona, 08028 Barcelona, Spain. Email: francesc.illas@ub.edu; Phone: +34-93-402-1229; Fax: +34-93-402-1231

† Electronic Supplementary Information (ESI) available: See DOI: 10.1039/x0xx00000x

various oxygen sites, even in small cluster model, is not reported yet. Therefore, understanding O_v in TiO_2 NPs would be interesting for applications as an efficient photocatalytic material.

The analysis of excess electron or Ti^{3+} centers is important to understand O_v in TiO_2 NP. From theoretical aspect, the computational methods based on density functional theory (DFT) have been chosen to describe diverse properties of many materials, but there are several serious problems that could be addressed depending on methodology. Actually, it is well known that DFT method using Perdew, Burke and Ernzerhof (PBE) functional,[40] one of the most commonly used DFT functional classified as Generalized Gradient Approximation (GGA) functionals, describes dispersive-unpaired electrons in order to reduce the Coulomb repulsion even in fully localized systems.[41-44] Owing to such kind of dispersive effect on unpaired electrons, abnormally strong delocalized solutions were obtained for reduced TiO_2 systems. Moreover, PBE functional gives underestimated band gap for TiO_2 systems. To solve these problems, usage of hybrid DFT functionals containing certain amount of Hartree-Fock exchange was suggested. Among many hybrid DFT functionals, B3LYP (20 %Fock)[45] and PBE0 (25 %Fock)[46] have been most widely used in theoretical studies. Even though hybrid functional properly described the presence of localized defect state on reduced TiO_2,[47] these popular hybrid functionals containing high amount of HF generally give the overestimated band gap of oxide semiconductors.[48]

Herein, we systemically investigate the properties of stoichiometric $(TiO_2)_{35}$ anatase NP and neutral single oxygen removed one. The bipyramidal $(TiO_2)_{35}$ NP, maintaining anatase structure after geometrical relaxation, seems to be a proper model to study the physical and electronic properties of oxygen vacancy in TiO_2 NP by comparing those of bulk and slab surface. Furthermore, the size (~ 2 nm) is also appropriate to rationalize the experimental result about TiO_2 NPs. Various oxygen vacant sites, representing the whole one, are examined according to position, coordination number (CN) and bond length with adjoined Ti. A modified PBE0 hybrid,[34] which is considered to be suitable to describe O_v properties of TiO_2 bulk, is used to compare with more popular functionals (PBE and PBE0). Unlike in the bulk material, the well-ordered TiO_2 anatase structure is partially changed for relatively high surface to volume ratio and also because of the appearance of some under-coordinated atoms (Ti_{4c}, Ti_{5c} and O_{1c}) in the nanoparticle. Moreover, oxygen vacancy formation energy (E_f^O) of the particular three-coordinated facet site is surprisingly small than those on other TiO_2 systems.

Computational detail

All calculations were carried out using the first-principles electronic structure theory based on DFT using all electron numerical atom-centered orbitals that is supplied by Fritz Haber Institute *ab initio* molecular simulations (FHI-aims) program package.[49] DFT calculations have been conducted by different hybrid functionals (the exact HF exchange is partly mixed-in with the DFT exchange) with tight grid and tier-1 basis set. We have used PBE (0 %Fock), modified PBE0 (12.5 %Fock, hereafter referred to as PBEx)[34] and PBE0 (25 %Fock) functionals in this study. PBEx functional was a newly devised one that contains the optimal %Fock confirmed by the calculated electronic structures and physical properties for O_v in TiO_2 bulk polymorphs.[34] PBE results would be less reliable in this O_v study, but the results of three functionals are presented in this paper to compare the functional effect in the description of TiO_2 NP properties. For the case of O_v, with two excess electrons, closed-shell singlet and open-shell triplet states were calculated and we analysed the result from the more stable one. The scalar-relativistic effects treated at the scaled zero-order regular with collinear spin (ZORA) level were taken into account. To optimize pristine and reduced NPs, the convergence criteria for geometry relaxations were set to 10^{-2} eV/Å.

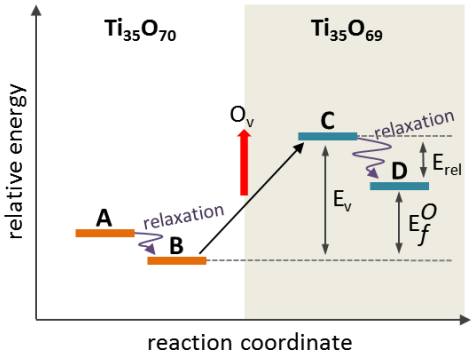

Fig. 1 The energy diagram according to O_v calculation sequence. **A** is initial bipyramidal TiO_2 NP ($Ti_{35}O_{70}$) modeled from TiO_2 anatase bulk structure and **B** is the optimized geometry of **A**. **C** ($Ti_{35}O_{69}$) has the same geometry as **B** with one oxygen removal. **D** is the optimized structure of **C**.

The oxygen vacancy formation energy (E_f^O) at various oxygen sites is calculated as:

$$E_f^O = E(Ti_{35}O_{69}) + \frac{1}{2}E(O_2) - E(Ti_{35}O_{70}) \quad (1)$$

where $E(Ti_{35}O_{70})$ and $E(Ti_{35}O_{69})$ are the total energies of the pristine and reduced TiO_2 NP that are fully relaxed structures using each functional, respectively. $E(O_2)$ is the energy of O_2 molecule in its triplet ground state. Herein, positive value of E_f^O stands for the extra energy required to form O_v. Fig. 1 shows the schematic energy diagram of O_v formation according to our calculation process. **A** is initial pristine, bulk cut, TiO_2 NP (**A** in Fig. 2) that is modeled from TiO_2 anatase bulk structure and **B** is the relaxed one. **C** is the single point geometry of $Ti_{35}O_{69}$ NP with one oxygen atom is removed from **B**. **D** is the optimized structure of **C**. Here, we define the following energetics.

$$E_f^O = E(\mathbf{D}) + \frac{1}{2}E(O_2) - E(\mathbf{B}) \quad (2)$$

$$E_v = E(\mathbf{C}) - E(\mathbf{B}) + \frac{1}{2}E(O_2) \quad (3)$$

$$E_{rel} = E_v - E_f^O = E(\mathbf{C}) - E(\mathbf{D}) \quad (4)$$

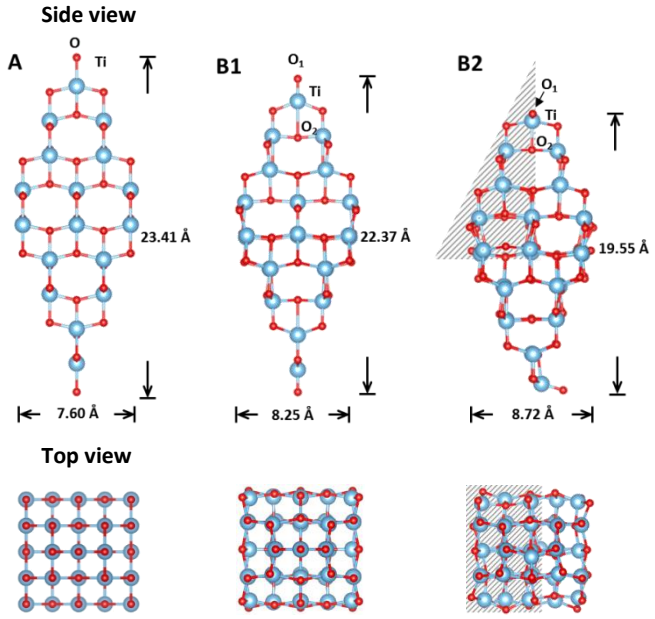

Fig. 2 Pristine TiO_2 NP structures are presented. Blue and red spheres denote titanium and oxygen atoms, respectively. Oxygen atoms marked in gray color represent the single oxygen vacancy site domain.

where E(**B**), E(**C**) and E(**D**) are the energy of **B**, **C** and **D** structures, respectively. Vertical energy (E_v) and relaxation energy (E_{rel}) are introduced to analyze E_f^O.

Results and discussion

Fig.2 shows the structures of pristine $(TiO_2)_{35}$. The TiO_2 NP was basically designed as the bipyramidal anatase structure (A) that was suggested by Barnard et al.[50] The initial structure was constructed by cutting {101} surface planes known to have the lowest surface energy for anatase TiO_2 polymorph. Thus, the strategy of designing NP follows the Wulff-construction method.[51] There are two different optimized geometries (denoted as B1 and B2) for **B** of $(TiO_2)_{35}$ NP. B1 coincides with the optimized geometry of TiO_2 NP in previous studies,[50, 52] where titanium atoms are relaxed inwards, oxygen atoms moves outward directions, and the O_1-Ti-O_2 is almost linear (with angle of 179.9°). However, Ti-O at both tips of B2 are bent to opposite sides (with angle O_1-Ti-O_2 of 113.2°) and titanium and oxygen atoms are more relaxed to each direction. As a result, the height of TiO_2 NP is more shortened and the width becomes wider than B1. To the best of our knowledge, B2 was not reported yet, but it is more stable than B1 by around 1.06 eV for all the DFT functionals used. Unlike TiO_2 bulk structure, the geometry of NP would easily change to decrease the higher surface to bulk ratio. In this study, the more stable B2 is adopted as TiO_2 NP structure (**B** in Fig. 1). In TiO_2 anatase bulk structure, axial Ti-O bond (Ti-O_{ax}, 2.01 Å) is longer than equatorial ones (Ti-O_{eq}, 1.94 Å) from DFT calculation (Fig. S1),[7, 28] which is slightly longer than experimental values (1.976 Å and 1.946 Å at 15 K).[53] Despite the lengths of Ti-O_{ax} and Ti-O_{eq} were set as 2.003 Å and 1.946 Å, respectively, in the initial geometry (A), brought from our previous study of TiO_2 anatase bulk structure,[34] the distance of terminal Ti-O_1 changed to 1.592 ~ 1.619 Å (depending on DFT functionals) and Ti-O_{ax} becomes shorter than Ti-O_{eq} around some 3-coordinated oxygen atoms (O_{3c}) in B2 structure. The symmetry of well-ordered TiO_2 anatase structure, consisting of Ti_{6c} and O_{2c}, is broken due to some under-coordinated titanium (Ti_{4c}, Ti_{5c}) and oxygen atoms (O_{1c}) and bent Ti-O_1 at tips.

Table 1 Geometrical parameters (height and width, in Å) and the energy values (in eV) of **HOMO**, **LUMO**, and HOMO-LUMO gap (ΔE_{H-L}) of B1 and B2.

		height	width	HOMO	LUMO	ΔE_{H-L}
PBE	straight tip (B1)	22.54	8.31	-7.41	-4.98	2.43
	bent tip (B2)	19.64	8.78	-7.45	-4.85	2.60
PBEx	straight tip (B1)	22.37	8.25	-8.19	-4.60	3.59
	bent tip (B2)	19.55	8.72	-8.27	-4.46	3.81
PBE0	straight tip (B1)	22.22	8.20	-9.00	-4.19	4.81
	bent tip (B2)	19.43	8.66	-9.08	-4.04	5.05

Table 1 lists the calculated geometrical parameters and energy values of $(TiO_2)_{35}$ NP depending on the structure types (B1 and B2) and DFT functional. The structural differences between B1 and B2 are similar in all DFT functionals used, as described above. In spite of the structural similarity, the energy gap between the highest occupied molecular orbital (HOMO) and the lowest unoccupied molecular orbital (LUMO) (ΔE_{H-L}) depends highly on the functionals, as expected. For comparison, the calculated energy values of bulk anatase TiO_2 are given in Table S1.[28, 34, 39, 66] Actually, ΔE_{H-L} is only an approximation to the band gap and the quality of approximation is determined by the calculation methods.[54] In the case of DFT, it depends on the exchange-correlation potential and the ratio of HF in functional.[55-57] Among the values of ΔE_{H-L}, the PBEx results are analogous with the experimental band gap of bulk anatase (3.20 eV[58-60]) and the TiO_2 NP (mixture of rutile and anatase phase; ca. 3.10 eV[61-63]). Moreover, previous studies reported that optical band gap of TiO_2 nanocrystal becomes large as crystal size decrease.[27, 64, 65] Therefore PBEx functional seems to be appropriate for the DFT calculation of TiO_2 NP on the basis of the calculated ΔE_{H-L} value. Hence, the structures and data calculated using PBEx are mainly presented for the sake of simplicity. Nevertheless, the results of PBE and PBE0 are included in the electronic supplementary information.

The properties of O_v in $(TiO_2)_{35}$ NP were investigated by one neutral oxygen atom removal from B2. Among total 70 oxygen atoms in the $(TiO_2)_{35}$ NP, there are 25 non-superimposible oxygen atoms by symmetry operation. Thus, 25 oxygen sites (marked in gray color in Fig. 2) were selected and removed one by one to examine the properties of single oxygen vacancy, which covers entire single oxygen vancancies. These vacancies were classified as tip (**T**), edge (**E**), facet (**F**),

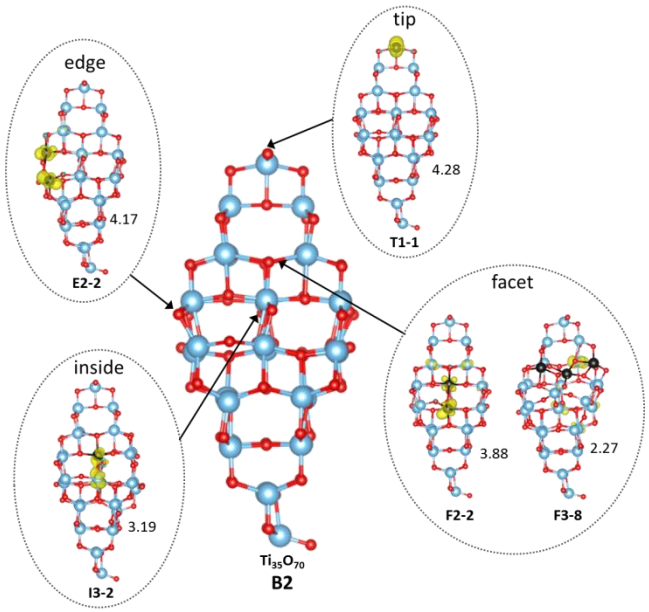

Fig. 3 Calculated structure of B2 and five representative structures for single oxygen vacant $Ti_{35}O_{69}$ NP (**D**) at various O_v sites. Yellow color shows the spin density in isosurface of 0.05 e·au^{-3}. Blue, red, and black spheres denote titanium, oxygen and first neighbored titanium atoms to the O_v site, respectively. E_f^O values in eV are also included.

and inside (**I**) type depending on the position of oxygen removed.

Fig. 3 displays the calculated structure of B2 and five representative sructures for single oxygen vacant $Ti_{35}O_{69}$ NP that were fully optimized after single oxygen atom removal from B2. These structures have the lowest E_f^O in each domain type (**T**, **E**, **F**, and **I**) of vacant oxygen atom sites depending on position and CN (Table 2). We name each single oxygen vacant state as Xm-n where X/m designates domain type/CN, and n is sequencially numbered accoring to the distance of the removed oxygen from the center of mass. For example, **F2-2** represents the oxygen vacant state where the oxygen second nearest from the center of mass and coordinated with two Ti atoms (CN=2) in facet domain was removed. The structures and energy values calculated using PBE and PBE0 functionals were presented in supporting information (Fig. S2 and S3). The spin densities are mainly distributed on d-orbital (mostly d_{z^2}, and partially $d_{x^2-y^2}$) and the degree of localization on the neighboring Ti atoms which are reduced to Ti^{3+} and the corresponding distribution of spin density varies with the functional, which is similar to previous studies.[28, 38] One should warn that when fully localized solutions are involved, possible low lying electronic isomers may exist which differ in the position of the Ti^{3+} cation in the NP. However, these have not been further considered here. As %Fock increases in the DFT functional (PBE < PBEx < PBE0), O_v from NP results in a solution that the spin density of two excess electrons are localized in some particular parts of NP. The excess electrons would initially move to the first-neighboring titanium atoms. In most cases, the spin density distribution is shown at these adjacent titanium atoms. Excess electrons stay at the only one nearest titanium atom in **T1-1**. For most of the reduced NPs with O_v at edge and facet domains, excess electrons remain at least one nearest Ti atom and one disperse to other Ti atoms or transferred to another firtst-neighboring Ti. The excess electrons are mainly localized at the closer Ti atoms from the vacant site among two or three adjoined Ti atoms. In all O_v states generated in Inside domain and several O_v states in Facet domain that result in the reduced NPs having relatively more deformed structure, electrons transfer to Ti sites at longer distance from the oxygen vacant site. The geometrical distortion concomitant with localized spin stabilization contributes to relatively high E_{rel} and thus decrease E_f^O. **I3-2** has the lowest E_f^O value from the PBE result, while **F3-8** from the PBEx and PBE0 results. This implies that the the effect of %Fock on the properties of O_v may be site dependent and highlights the importance of using a DFT method properly describing as many properties of these materials as possible.

Reorganization of the structure around the vacant space (distance to neighboring titanium atoms) and the presence of two excess electrons induced by O_v would be major factors in the relaxation of the reduced TiO_2 NP. The optimized structures and the lowest E_f^O sites are different depending on

Table 2 Calculated (PBEx) values (in eV) of vertical energy (E_v), relaxation energy (E_{rel}), oxygen vacancy formation energy (E_f^O), and energy level of oxygen vacancy defect state below LUMO (S_v-**1** and S_v-**2**). All values are lined up in order of vacant oxygen atom distance from center of mass within each classification. In each classification, the lowest E_f^O value words in bold type.

position	CN[a]	site[b]	E_v	E_{rel}	E_f^O	S_v-1	S_v-2
tip	1	T1-1	4.54	0.26	**4.28**	0.47	0.64
edge	2	E2-1	5.87	1.38	4.49	0.81	1.64
		E2-2	5.97	1.79	**4.17**	1.02	1.75
		E2-3	5.97	1.61	4.37	0.84	1.85
		E2-4	5.77	1.19	4.58	0.75	0.95
		E2-5	6.14	1.27	4.87	0.72	1.55
		E2-6	5.86	1.44	4.42	1.00	1.39
		E2-7	5.98	0.83	5.15	0.84	1.74
facet	2	F2-1	5.47	1.53	3.94	0.68	1.28
		F2-2	5.29	1.40	**3.88**	0.68	1.28
		F2-3	6.01	1.57	4.44	0.74	1.69
	3	F3-1	5.91	1.54	4.37	0.84	1.85
		F3-2	6.03	1.76	4.27	0.55	1.78
		F3-3	6.02	1.51	4.51	0.73	1.75
		F3-4	6.23	2.03	4.21	1.09	1.43
		F3-5	6.92	2.02	4.89	1.02	1.10
		F3-6	6.36	1.71	4.65	0.86	1.71
		F3-7	6.63	1.50	5.13	1.20	1.32
		F3-8	6.48	4.21	**2.27**	0.71	1.17
		F3-9	5.12	0.73	4.39	1.84	
		F3-10	5.63	0.84	4.79	1.65	
inside	3	I3-1	6.14	1.86	4.28	1.22	1.87
		I3-2	5.76	2.57	**3.19**	0.96	1.15
		I3-3	6.09	2.87	3.23	0.94	1.10
		I3-4	6.06	1.91	4.15	0.93	2.06

[a] **CN** is number of first neighboring titanium atoms to removed oxygen atom.
[b] **site** is designated as combination of position, CN, and the order of vacant oxygen atom distant from center of mass.

the exchange functionals because the distribution of two excess electrons is strongly affected by the amount of non-local HF exchange. Table 2 lists the values of E_v [eq. (3)], E_{rel} [eq. (4)], E_f^O [eq. (2)], and energy level of oxygen vacancy defect state below LUMO (S_v-1 and S_v-2) as calculated using PBEx functional. The data from PBE and PBE0 functionals is listed in Table S2. E_v generally increases with CN regardless of functional; the sites having the highest and lowest E_v are tip (**T1-1**) and 3-coordinated facet (PBE: **F3-8**, PBEx and PBE0: **F3-5**), respectively. However, the tendency of E_{rel} is quite different according to the functional due to the two factors, geometrical relaxation and distribution of excess electrons, which influence relaxation of reduced NP.

The range of E_f^O is 2.81 ~ 5.61 eV in PBE, 2.27 ~ 5.46 eV in PBEx and 2.05 ~ 5.12 eV in PBE0; all functionals provide a similar qualitative picture but with some remarkable differences as well. The average value (PBE: 4.19, PBEx: 4.28, PBE0: 4.16 eV) is quite close to E_f^O in TiO_2 Bulk (Table S1),[28, 34, 39, 66] but it is much lower when the O atom is removed from some specific sites. This is because of the relaxation of the reduced TiO_2 system upon vacancy formation which varies depending on the features of O_v site that is determined by the influence of vacant space and excess electron on surrounding titanium atoms. In the reduced anatase TiO_2 bulk, there is only single type (3-coordinated one) of O_v site and the relaxation effects were smaller than in the TiO_2 NP; [32, 34] atoms surrounding vacant site maintained pristine TiO_2 structure, and excess electrons were distributed over the three Ti atoms directly adjacent to the O_V site. For comparison, dissociation energy of O_2 molecule was calculated using three functionals. The value (PBE: 6.77 eV, PBEx: 7.69 eV, PBE0: 8.62eV) increases as %Fock increases. Fig. S4 presents the changes of E_f^O against vacant oxygen atom distance from center of mass. The range of E_f^O, except for particulary low E_f^O (**F3-8**) in PBEx and PBE0 results, is narrowed as %Fock increases. As % Fock decreases, the localized and delocalized characters of the excess electrons are mixed, and the range of E_f^O becomes broader. Even the same (3)-coordinated oxygen atoms have led to different features when the O_v is formed in the TiO_2 NP. The oxygen sites having the lowest E_f^O are **I3-2** in PBE, and **F3-8** in PBEx and PBE0. It is worth pointing out that the situation here is different from the O_v tendency in ceria (CeO_2) NPs[67, 68] where removal of a low (2)-coordinated oxygen requires the lowest energy. Interestingly, however, high (3)-coordinated oxygen sites have the lowest E_f^O in TiO_2 NP because relaxation effect is quite large. According to the definition of E_f^O in eq. (2), the value of E_f^O decreases as the E_v decreases and E_{rel} increases. Although **T1-1** is the outermost site, E_f^O is quite high as 4.28 eV because of the lowest E_{rel} (0.26 eV). The **F3-8** as the most stable O_v site is coincident with previous result that the subsurface O_v (CN=3) is more stable than the surface O_v (CN=2) in TiO_2 anatase slabs from the calculation of E_f^O for different surface and subsurface sites in various TiO_2 slab models using the hybrid DFT functionals;[36] a feature which is also in agreement with experiment.[17]

In order to understand the reason of **F3-8** site having the lowest E_f^O in PBEx and PBE0 calculations, we carefully analyzed

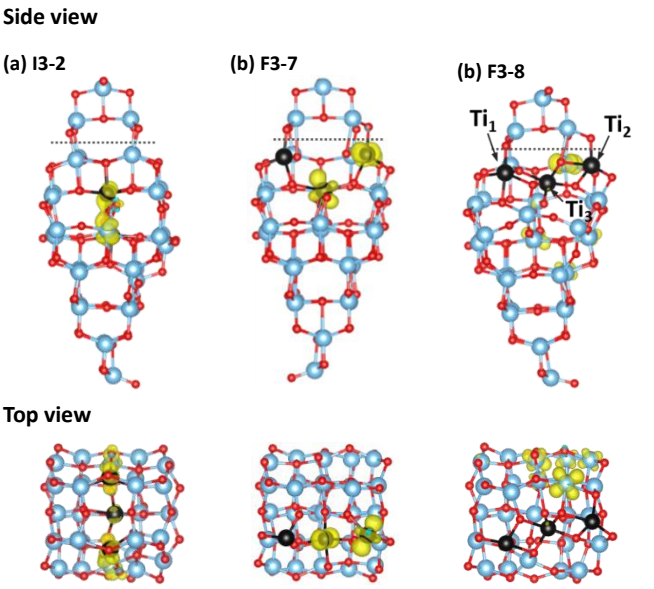

Fig. 4 PBEx calculated structures of $Ti_{35}O_{69}$ NP with oxygen removed at three O_{3c} sites that where Ti-O_{ax} is shorter than the two Ti-O_{eq} distances. The isovalue of spin density is 0.05 e·au^{-3}. For clarity, atoms above the dotted line were removed in top view structures.

the geometrical differences between each of oxygen sites in optimized pristine TiO_2 NP. Normally, the O_{3c} has two short Ti-O_{eq} (ca. 1.94 Å) and one long Ti-O_{ax} (ca. 2.01 Å) in bulk anatase lattice,[7, 28] as shown in Fig. S1. However, among 14 O_{3c} sites, we found that, in the pristine NP, only three O_{3c} sites showed that Ti-O_{ax} is shorter than two Ti-O_{eq}. The reduced NPs with oxygen removed at these O_{3c} sites were shown in Fig. 4 (PBE and PBE0 results are in Fig. S5). The lengths of Ti-O_{ax} and Ti-O_{eq} at three sites (**I3-2**, **F3-7** and **F3-8**) are listed in Table S3. At **I3-2**, Ti-O_{ax} is shorter than two analogous-lengths Ti-O_{eq}. In other words, though Ti-O_{ax} shortens, O_{3c} is still symmetrically located from both side titanium atoms. In reduced TiO_2 NP, the vacant space remains after relaxation and excess electrons tend to spread to surface along nearest-neighboring titanium atoms. It was found that the spin density is localized at low-coordinated surface titanium atoms as the %Fock increases.

However, more complicated structural features appear for the reduced NP with O_v at **F3-7** (b) and **F3-8** (c). Even though these two facet sites are opposite in approximately symmetrical TiO_2 NP structure, the properties of O_v are quite different. At **F3-7**, vacant space is maintained and excess electrons are localized at two closer titanium atoms among three nearby titanium atoms, which is similar to the results at other O_{3c} sites. On the other hand, at **F3-8**, the location of atoms surrounding O_v site changes obviously and two of three adjacent titanium atoms (black spheres) form additional coordination with nearby oxygen atom. In other words, after O_v formation, Ti_1 and Ti_2 are additionally coordinated with nearby oxygen atom and only Ti_3 loses 1 CN through large geometrical change. Thus, CNs of Ti_1, Ti_2, and Ti_3 are 5, 5, and 6 in pristine NP and 5, 5, and 5 in reduced NP, respectively. At the PBEx level of theory, one excess electron is localized at next-neighboring titanium atom and the other is delocalized at

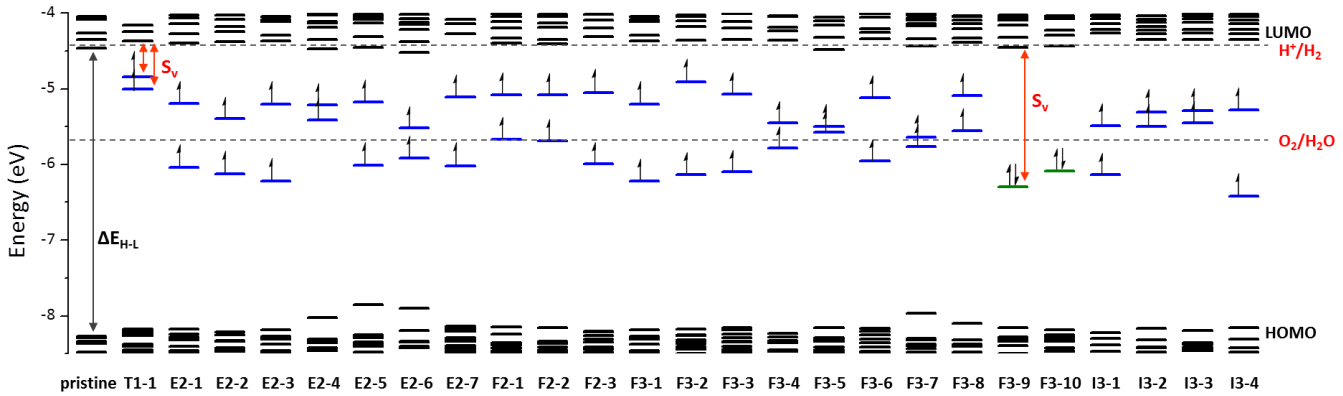

Fig. 5 Kohn-Sham orbitals energy level diagram of $Ti_{35}O_{69}$ NPs and $Ti_{35}O_{70}$. The triplet state energy levels are for spin-up eigenvalues. The dotted lines indicate the standard redox potentials for water splitting at pH = 0. The singly occupied and doubly occupied defect states are denoted in blue and green for triplet and singlet states, respectively. Other occupied and unoccupied molecular orbitals are shown in black.

opposite side surface titanium atoms that is next to the spin delocalized one. In PBE0 results, one electron stays at Ti_3 and the other is localized at next neighboring surface titanium atom. However, unlike PBEx and PBE0, PBE functional could not appropriately predict the distinct features of O_v at **F3-8**. The empty space still remains (each adjacent titanium atom loses 1 CN and keeps 5 CN), the geometrical change is less noticeable and the excess electrons migrate to surface titanium atoms. It means that the reduced NP structure is strongly altered by the description of excess electrons. Though spin density distribution was different in PBEx and PBE0, it is important to highlight that the large relaxation effect at **F3-8** site was predicted with both functionals.

One distinct difference between **F3-7** and **F3-8** sites is the dangling oxygen atom bending toward **F3-8**; for this reason, O_{3c} geometry seems to be much deformed at **F3-8**. Thus, we argue that the relaxation of oxygen vacant structure would be affected by the geometrical singularity of pristine TiO_2 anatase NP, in which the normal O_{3c} structure is broken and Ti-O of both tips are asymmetrically bent to opposite sides. At **F3-8** site, E_{rel} is predominantly large, and E_f^O is the lowest. In other words, **F3-8** would be the most preferred O_v site from thermodynamic point of view. The geometrical change and localization of spin density are consistent with polaronic effect accompanying excess electron in reduced TiO_2 surface; excess electrons by O_v are localized near the surface vacant site and lattice distortion is induced in polaronic (delocalized) solution.[17, 69]

The presence of Ti^{3+} ions in reduced TiO_2 system was confirmed by band gap narrowing that results from the electronic structure change induced by the O_v.[23, 25-27] The defect state appeared at around 1 eV below the conduction band minimum (CBM) from the experimental results in TiO_2 systems.[27] Fig.5 presents molecular orbitals energy level diagram of $Ti_{35}O_{69}$ NP at 25 O_v sites (PBE and PBE0 results are in Fig. S6). The defect states are presented as singly (triplet state) or doubly (singlet state) occupied molecular orbital. Because molecular orbital energy levels of up- and down-spin in triplet states were very similar except for defect states, only up-spin eigenvalues are presented. The spin-unrestricted triplet state was dominantly more stable than the closed-shell singlet one in most of the reduced TiO_2 NPs. It clearly showed that the defect states exist between HOMO and LUMO level and the values of ΔE_{H-L} and S_v vary with O_v site and functional. Not only ΔE_{H-L} but also S_v increased with the increasing amount of %Fock in reduced TiO_2 NPs. The range S_v is 0.01 ~ 0.83 eV in PBE, 0.47 ~ 2.06 eV in PBEx and 1.42 ~ 3.32 eV in PBE0 and the results of PBEx are best matched to the experimental values. The position of the HOMO and LUMO energy levels was also changed upon O_v formation. These changes allow for new electronic transitions from both HOMO and defect states to LUMO, and from HOMO to defect states. For this reason, oxygen vacancy leads to bandgap narrowing of TiO_2 NPs, which would be responsible for visible light absorption. Furthermore, in comparison with the standard redox potentials for water splitting (at pH = 0),[2, 70-72] the HOMO level must be located below the oxygen evolution (OER) potential (O_2/H_2O), whereas LUMO level must exceed the hydrogen evolution reduction (HER) potential (H^+/H_2). LUMO positioned close to HER potential and defect state appeard near to OER potential could make reduced TiO_2 NPs as promising candidates for photocatalytic water splitting. In the aspect of redox potential, 17-like sites would be suitable for photocatalyst, but the defect states of O_v sites having low E_f^O (F3-8 and I3-2) are higher than OER potential. However, the correlation between O_v sites and photocatalytic activity was not shown. Actually, these results are not enough to be convinced that oxygen removed TiO_2 NPs can be applied to visible light adsorbing photocatalyst for water spliting. Future work should therefore include a more systematic study of reduced TiO_2 NPs in solution, the dynamics of photoexcited state of reduced TiO_2 NPs, O_v site migration behavior, and multi-oxygen vacancy effect.

Conclusions

We investigated the properties of neutral single oxygen vacancy in $(TiO_2)_{35}$ anatase nanoparticle focusing on the effect of the different possible vacant sites by DFT calculations using various DFT methods including hybrid functionals. Oxygen sites in $(TiO_2)_{35}$ are classified by position with respect to the center

of mass, coordination number and bond length with first-neighboring Ti. We examined 25 oxygen sites that could represent whole oxygen sites under symmetry operations. Atomic and electronic structures of pristine and reduced TiO_2 nanoparticles were obtained using PBE based hybrid functionals; PBE (0 %Fock), PBE0 (25 %Fock), and newly defined PBEx (12.5 %Fock).[34] Slightly differently from bulk structure, upon oxygen vacancy formation, the symmetry is broken and the two dangling oxygen atoms at both tips are bent to opposite sides due to high surface to bulk ratio and some under-coordinated atoms (Ti_{4c}, Ti_{5c} and O_{1c}) in nanoparticle. The properties of oxygen vacancy in the $(TiO_2)_{35}$ nanoparticle depend on vacant site and %Fock of the functional used.

Oxygen vacancy formation energy and the band edge energy levels of the defect state are quite dependent on vacant sites. Energetically most favourable oxygen atom for vacancy formation from nanoparticle is high (three)-coordinated one in facet domain which is in contrast with results reported for ceria nanoparticles.[67, 68] This is because the relaxation energy is largest at the particular facet site of which 3-coordinated structure with surrounding titanium atoms is broken from normal one in TiO_2 anatase system. The result predicted by the PBEx functional corresponds to HOMO-LUMO gap of pristine nanoparticle of 3.81 eV and defect state of reduced nanoparticle in the 0.47 ~ 2.06 eV range below LUMO energy level.

Finally, our study shows that introducing one O vacancy in the $(TiO_2)_{35}$ anatase nanoparticle gives rise to significant differences in the pristine and reduced structure in comparison with bulk system. Moreover, oxygen vacancy formation energy (2.27 eV) is surprisingly small compared with that of bulk or slab surface, and the energies of defect states induced by O vacancy are close to oxygen evolution potential. These could provide an evidence of the importance of the oxygen vacancy of TiO_2 nanoparticles for efficient photocatalyst.

Acknowledgements

This work was supported by the South Korea Ministry of Education, Science and Technology, subjected to the project EDISON (Education-research Integration through Simulation On the Net, Grant No.: 2012M3C1A6035359, by Spanish MINECO CTQ2015-64618-R grants and, in part by Generalitat de Catalunya grants 2014SGR97 and XRQTC. This project has received funding from the EU Horizon 2020 research under the NOMAD Excellence Center (grant Number 676580). K. C. K. is grateful to the Basic Science Research Program through the National Research Foundation of Korea (NRF) funded by the Ministry of Education (NRF-2014R1A6A3A03056449), and F.I. acknowledges additional support from the 2015 ICREA Academia Award for Excellence in University Research.

References

1 I. Justicia, P. Ordejón, G. Canto, J. L. Mozos, J. Fraxedas, G. A. Battiston, R. Gerbasi and A. Figueras, *Adv. Mater.* , 2002, **14**, 1399-1402.
2 M. Ni, M. K. H. Leung, D. Y. C. Leung and K. Sumathy, *Renew. Sustainable Energy Rev.*, 2007, **11**, 401-425.
3 U. Bach, D. Lupo, P. Comte, J. E. Moser, F. Weissortel, J. Salbeck, H. Spreitzer and M. Gratzel, *Nature*, 1998, **395**, 583-585.
4 N. G. Park, J. van de Lagemaat and A. J. Frank, *J. Phys. Chem. B*, 2000, **104**, 8989-8994.
5 M. Gratzel, *Nature*, 2001, **414**, 338-344.
6 S. Na-Phattalung, M. F. Smith, K. Kim, M.-H. Du, S.-H. Wei, S. B. Zhang and S. Limpijumnong, *Phys. Rev. B*, 2006, **73**, 125205.
7 C. Di Valentin, G. Pacchioni and A. Selloni, *Chem. Mater.*, 2005, **17**, 6656-6665.
8 N. Serpone, *J. Phys. Chem. B*, 2006, **110**, 24287-24293.
9 C. Di Valentin, G. Pacchioni and A. Selloni, *J. Phys. Chem. C*, 2009, **113**, 20543-20552.
10 S. A. Shevlin and S. M. Woodley, *J. Phys. Chem. C*, 2010, **114**, 17333-17343.
11 T. Sekiya, T. Yagisawa, N. Kamiya, D. Das Mulmi, S. Kurita, Y. Murakami and T. Kodaira, *J. Phys. Soc. Jpn.*, 2004, **73**, 703-710.
12 S. Wendt, P. T. Sprunger, E. Lira, G. K. H. Madsen, Z. Li, J. Ø. Hansen, J. Matthiesen, A. Blekinge-Rasmussen, E. Lægsgaard, B. Hammer and F. Besenbacher, *Science*, 2008, **320**, 1755-1759.
13 A. Naldoni, M. Allieta, S. Santangelo, M. Marelli, F. Fabbri, S. Cappelli, C. L. Bianchi, R. Psaro and V. Dal Santo, *J. Am. Chem. Soc.*, 2012, **134**, 7600-7603.
14 X. Pan, M.-Q. Yang, X. Fu, N. Zhang and Y.-J. Xu, *Nanoscale*, 2013, **5**, 3601-3614.
15 H. Zhang and J. F. Banfield, *J. Mater. Chem.*, 1998, **8**, 2073-2076.
16 M. R. Ranade, A. Navrotsky, H. Z. Zhang, J. F. Banfield, S. H. Elder, A. Zaban, P. H. Borse, S. K. Kulkarni, G. S. Doran and H. J. Whitfield, *Proc. Natl. Acad. Sci. U. S. A.*, 2002, **99**, 6476-6481.
17 M. Setvin, C. Franchini, X. Hao, M. Schmid, A. Janotti, M. Kaltak, C. G. Van de Walle, G. Kresse and U. Diebold, *Phys. Rev. Lett.*, 2014, **113**, 086402.
18 L. Sang, Y. Zhao and C. Burda, *Chem. Rev.*, 2014, **114**, 9283-9318.
19 Z.-w. Qu and G.-J. Kroes, *J. Phys. Chem. B*, 2006, **110**, 8998-9007.
20 Z.-w. Qu and G.-J. Kroes, *J. Phys. Chem. C*, 2007, **111**, 16808-16817.
21 S. Li and D. A. Dixon, *J. Phys. Chem. A*, 2008, **112**, 6646-6666.
22 D. Cho, K. C. Ko, O. Lamiel-Garcia, S. T. Bromley, J. Y. Lee and F. Illas, *J. Chem. Theory Comput.*, 2016, DOI: 10.1021/acs.jctc.6b00519.
23 M. Nolan, S. D. Elliott, J. S. Mulley, R. A. Bennett, M. Basham and P. Mulheran, *Phys. Rev. B*, 2008, **77**, 235424.
24 J. Nerlov, S. V. Christensen, S. Weichel, E. H. Pedersen and P. J. Møller, *Surf. Sci.*, 1997, **371**, 321-336.
25 M. A. Henderson, W. S. Epling, C. H. F. Peden and C. L. Perkins, *J. Phys. Chem. B*, 2003, **107**, 534-545.
26 N. D. Abazović, M. I. Čomor, M. D. Dramićanin, D. J. Jovanović, S. P. Ahrenkiel and J. M. Nedeljković, *J. Phys. Chem. B*, 2006, **110**, 25366-25370.
27 F. Fabbri, F. Detto, N. Armani, N. Satoh, T. Besagni, M. Pavesi and G. Salviati, *J. Phys. Chem. C*, 2013, **117**, 3729-3738.
28 E. Finazzi, C. Di Valentin, G. Pacchioni and A. Selloni, *J. Chem. Phys.*, 2008, **129**, 154113.
29 G. Mattioli, F. Filippone, P. Alippi and A. Amore Bonapasta, *Phys. Rev. B*, 2008, **78**, 241201.

30 A. Janotti, J. B. Varley, P. Rinke, N. Umezawa, G. Kresse and C. G. Van de Walle, *Phys. Rev. B*, 2010, **81**, 085212.
31 B. J. Morgan and G. W. Watson, *J. Phys. Chem. C*, 2010, **114**, 2321-2328.
32 P. Deák, B. Aradi and T. Frauenheim, *Phys. Rev. B*, 2012, **86**, 195206.
33 H.-Y. Lee, S. J. Clark and J. Robertson, *Phys. Rev. B*, 2012, **86**, 075209.
34 K. C. Ko, O. Lamiel-Garcia, J. Y. Lee and F. Illas, *Phys. Chem. Chem. Phys.*, 2016, **18**, 12357-12367.
35 M. wang, M. Feng and Y. Lu, *Mod. Phys. Lett. B*, 2014, **28**, 1450076.
36 H. Li, Y. Guo and J. Robertson, *J. Phys. Chem. C*, 2015, **119**, 18160-18166.
37 B. J. Morgan and G. W. Watson, *Phys. Rev. B*, 2009, **80**, 233102.
38 S. Taizo, Y. Kenji, M. Susanne and S. Biplab, *J. Phys.: Condens. Matter*, 2012, **24**, 435504.
39 P. Deák, J. Kullgren and T. Frauenheim, *Phys. Status Solidi RRL*, 2014, **8**, 583-586.
40 J. P. Perdew, K. Burke and M. Ernzerhof, *Phys. Rev. Lett.*, 1996, **77**, 3865-3868.
41 M. Sodupe, J. Bertran, L. Rodríguez-Santiago and E. J. Baerends, *J. Phys. Chem. A*, 1999, **103**, 166-170.
42 J. Lægsgaard and K. Stokbro, *Phys. Rev. B*, 2000, **61**, 12590-12593.
43 M. Magagnini, P. Giannozzi and A. Dal Corso, *Phys. Rev. B*, 2000, **61**, 2621-2625.
44 I. de P. R. Moreira, F. Illas and R. L. Martin, *Phys. Rev. B*, 2002, **65**, 155102.
45 J. P. Perdew, M. Ernzerhof and K. Burke, *J. Chem. Phys.*, 1996, **105**, 9982-9985.
46 C. Adamo and V. Barone, *J. Chem. Phys.*, 1999, **110**, 6158-6170.
47 C. Di Valentin, G. Pacchioni and A. Selloni, *Phys. Rev. Lett.*, 2006, **97**, 166803.
48 M. Gerosa, C. E. Bottani, L. Caramella, G. Onida, C. Di Valentin and G. Pacchioni, *Phys. Rev. B*, 2015, **91**, 155201.
49 V. Blum, R. Gehrke, F. Hanke, P. Havu, V. Havu, X. Ren, K. Reuter and M. Scheffler, *Comput. Phys. Commun.*, 2009, **180**, 2175-2196.
50 A. S. Barnard, S. Erdin, Y. Lin, P. Zapol and J. W. Halley, *Phys. Rev. B*, 2006, **73**, 205405.
51 G. Wulff, *Z. Kristallogr. Material.*, 1901, **34**, 449-530.
52 L. Yinkai, L. Huijun and X. Wei, *Modelling Simul. Mater. Sci. Eng.*, 2010, **18**, 025004.
53 J. K. Burdett, T. Hughbanks, G. J. Miller, J. W. Richardson and J. V. Smith, *J. Am. Chem. Soc.*, 1987, **109**, 3639-3646.
54 J.-L. Bredas, *Mater. Horiz.*, 2014, **1**, 17-19.
55 F. Labat, P. Baranek, C. Domain, C. Minot and C. Adamo, *J. Chem. Phys.*, 2007, **126**, 154703.
56 C. J. Cramer and D. G. Truhlar, *Phys. Chem. Chem. Phys.*, 2009, **11**, 10757-10816.
57 G. Fazio, L. Ferrighi and C. Di Valentin, *J. Phys. Chem. C*, 2015, **119**, 20735-20746.
58 H. Minoura, M. Nasu and Y. Takahashi, *Ber. Bunsenges. Phys. Chem.*, 1985, **89**, 1064-1069.
59 L. Kavan, M. Grätzel, S. E. Gilbert, C. Klemenz and H. J. Scheel, *J. Am. Chem. Soc.*, 1996, **118**, 6716-6723.
60 D. Reyes-Coronado, G. Rodríguez-Gattorno, M. E. Espinosa-Pesqueira, C. Cab, R. d. Coss and G. Oskam, *Nanotechnology*, 2008, **19**, 145605.
61 S. Kalathil, M. M. Khan, S. A. Ansari, J. Lee and M. H. Cho, *Nanoscale*, 2013, **5**, 6323-6326.
62 Q. Kang, J. Cao, Y. Zhang, L. Liu, H. Xu and J. Ye, *J. Mater. Chem. A*, 2013, **1**, 5766-5774.
63 M. M. Khan, S. A. Ansari, D. Pradhan, M. O. Ansari, D. H. Han, J. Lee and M. H. Cho, *J. Mater. Chem. A*, 2014, **2**, 637-644.
64 S. Monticone, R. Tufeu, A. V. Kanaev, E. Scolan and C. Sanchez, *Appl. Surf. Sci.*, 2000, **162–163**, 565-570.
65 L. Ming, C. Kui, W. Wenjian, S. Chenlu, D. Piyi, S. Ge, X. Gang and H. Gaorong, *J. Phys. D: Appl. Phys.*, 2009, **42**, 105414.
66 T. Yamamoto and T. Ohno, *Phys. Chem. Chem. Phys.*, 2012, **14**, 589-598.
67 A. Migani, G. N. Vayssilov, S. T. Bromley, F. Illas and K. M. Neyman, *J. Mater. Chem.*, 2010, **20**, 10535-10546.
68 A. Migani, G. N. Vayssilov, S. T. Bromley, F. Illas and K. M. Neyman, *Chem. Commun.* , 2010, **46**, 5936-5938.
69 N. A. Deskins and M. Dupuis, *Phys. Rev. B*, 2007, **75**, 195212.
70 W.-J. Chun, A. Ishikawa, H. Fujisawa, T. Takata, J. N. Kondo, M. Hara, M. Kawai, Y. Matsumoto and K. Domen, *J. Phys. Chem. B*, 2003, **107**, 1798-1803.
71 T. Hisatomi, J. Kubota and K. Domen, *Chem. Soc. Rev.*, 2014, **43**, 7520-7535.
72 A. K. Singh, K. Mathew, H. L. Zhuang and R. G. Hennig, *J. Phys. Chem. Lett.*, 2015, **6**, 1087-1098.

